Modal Analysis and Ground Motion Modification for Tunnel Seismic Design in Fault Zone

R.A. Primadika[1*], T.F. Fathani[1], F. Faris[1]
[1]Department of Civil and Environmental Engineering, Gadjah Mada University, Yogyakarta, INDONESIA
*Corresponding author: ridhwanafnan@mail.ugm.ac.id

ABSTRACT

Tunneling in fault zones presents unique challenges, especially in seismically active regions like Indonesia. Faults can reduce the seismic performance of tunnels. This study aimed to analyze the impact of faults on the tunnel's modal behavior and develop a set of modified ground motion records for seismic tunnel design through fault zones. The Bener Dam diversion tunnel was used as a case study. A two-step analysis was conducted: (1) determining the tunnel's natural periods using modal analysis and (2) selecting and modifying ground motion records based on Indonesian seismic standards. Modal analysis indicated that the fault slightly increased the modal periods of the tunnel and significantly affected its mode shapes. Then, 11 pairs of ground motion records were selected considering earthquake magnitude and distance, the structure's natural periods, and the site S-wave velocity. The best records that matched the site were at CHY102 station (shallow crustal), KAWAI-N (benioff), and abashiri-g (megathrust). After modification, the highest PGA values were 0.44 g at CHY035 (shallow crustal), 0.40 g at KUJI-S (benioff), and 0.41 g at ROC1 (megathrust). These results highlight the importance of fault modeling for a proper ground motion selection and modification for accurate seismic analysis for tunnel design.

Keywords: Earthquake-Resistant Tunnel, Tunnel Through Fault, Natural Periods of Tunnels, Earthquake Modification.

1 INTRODUCTION

Tunneling in fault zones presents different problems compared to usual tunnels. The fault fracture zone in the tunnel can reduce the stability of surrounding rocks in tunnels (Wang *et al*., 2017). Seismic hazard and unfavorable geologic conditions, such as faults, can lead to unsatisfactory seismic performance (Hung *et al*., 2009). Most of the heavier tunnel damages during earthquake also occurred when the tunnel was across an unstable ground including ruptured fault plane (Wang, 1993). This reduction of tunnel seismic performance due to fault can lead to unsatisfactory design against earthquakes, especially in high seismic activity regions such as Indonesia. These large seismic activities are caused by four main plates surrounding the nation: the Eurasian Plate, the Indo-Australian Plate, the Philippine Sea Plate, and the Pacific Plate (National Earthquake Study Center of Indonesia, 2017).

Due to the reasons above, tunnels that pass through fault zones need to be designed to withstand earthquake loading. The methods that are often used in tunnel seismic design are pseudostatic analysis, response spectrum analysis, and time history dynamic analysis (Hung *et al*., 2009). For tunnel through faults, the commonly used method is to estimate the fault's displacements and then apply them as displacement loads to the tunnel (Hung *et al*., 2009). However, this method is difficult to perform due to the very high uncertainty. A proper non-linear acceleration time history analysis is able to consider the complex dynamic behavior of soil and the soil-structure interaction of tunnels (Amrei *et al*., 2020).

For dynamic time history analysis, earthquake time history records are necessary. Due to limited access to earthquake records in Indonesia, this kind of analysis is often done using records from other regions. These records need to be selected and modified according to the site characteristics of the designed structures. However, there are no specific standards of ground motion selection and modification for tunnel structures. Thus, making it difficult to be performed.

Another difference between other structures and tunnels is the method used to determine their natural periods. The natural periods of structure are necessary for ground motion modification. For underground structures such as tunnels, the surrounding soil and geological structures will affect their natural periods. This happens because, as the ground is deformed by the traveling waves, any tunnel structure in the ground will also be deformed (Hung *et al*., 2009). Wang (1993) proposed a method to consider the natural period of the soil as the tunnel's natural period, but this method cannot consider the influence of faults. Therefore, a method that can consider the geometry, mass, and stiffness of the tunnels and the rock mass is needed. One of the methods that is able to do this is modal analysis.

One of the cases of tunneling through faults in Indonesia was the Bener Dam diversion tunnel. In the planning process, the faults had not been discovered. So, the diversion tunnel had been designed without considering the effect of the faults (Bagio, 2021). Bagio (2021) also stated that, according to pseudostatic analysis, the tunnel was less stable under seismic loading. Thus, a further analysis was necessary.

This study aimed to analyze the impact of faults on tunnel modal behavior and develop a set of modified time history records for the Bener Dam diversion tunnel in compliance with Indonesian design codes. The approach involved determining the tunnel's natural periods through modal analysis, followed by selecting and modifying ground motion records based on applicable Indonesian standards. The modal analysis results, including natural periods and mode shapes, were utilized to assess the fault's influence on the tunnel's free vibration behavior.

2 SITE CONDITION

The site was located in Guntur Village, Bener District, Purworejo Regency, Central Java. Geographically, the Dam location was 7°35'54.5" S dan 110°1'12.84" E. The tunnel was already constructed and currently functioned to secure the construction site from the Bogowonto River. The tunnel would also function as an intake waterway for the power plant. The length of the tunnel was 935.8 m. The research was focused on the location near the fault, around 120 – 220 m from the tunnel inlet. The location is shown in Figure 1.

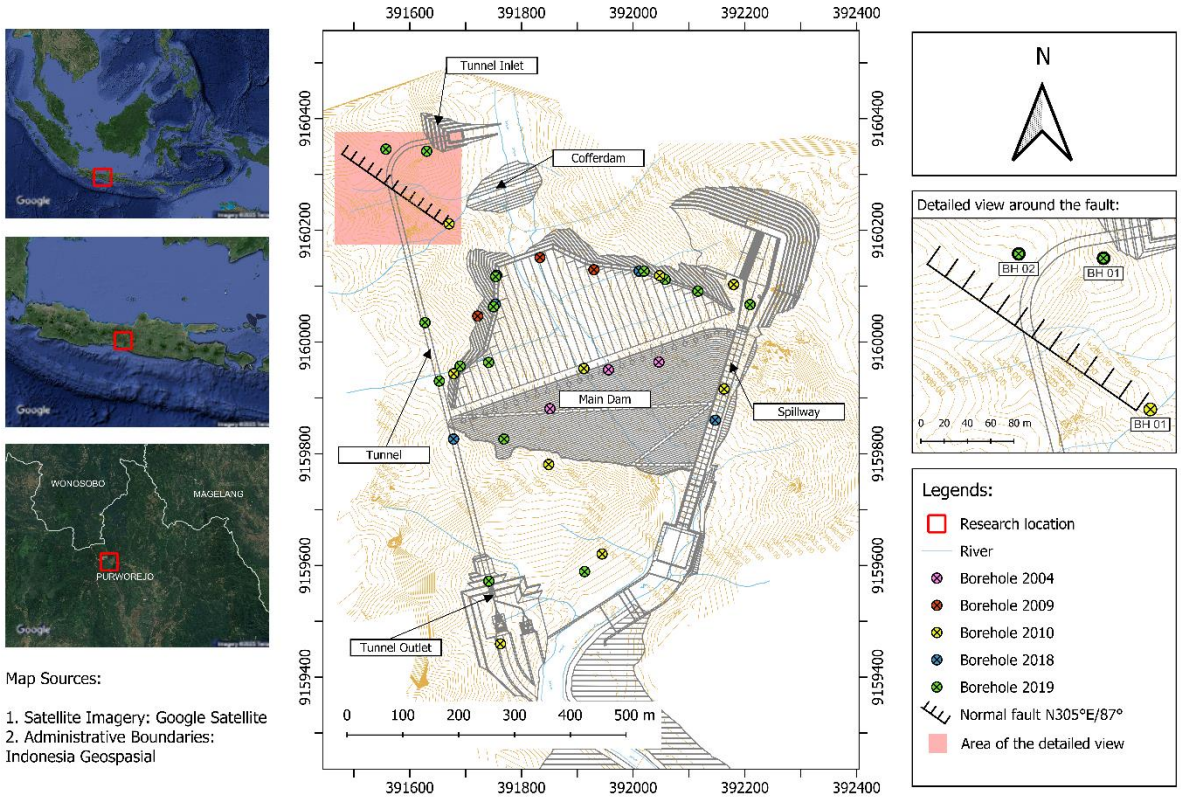

Figure 1. Site condition.

The geological formations comprising the Bener Dam diversion tunnel included Monomic Breccia, which could be classified into specific engineering geological units such as Monomic Breccia Matrix, Andesite Fragments, Tuff Fragments, and Polymic Breccia Matrix (Triristanto, 2023). The condition of rock mass quality on the site was controlled by geologic structures, more particularly faults, and some of them had cut the tunnel geometry (Sasangka, 2019). The fault considered in this study was identified as an inactive fault (Bagio, 2021).

3 METHODS

This study consisted of two steps: the first step was the determination of natural periods of the tunnel and the second step was the ground motion selection and modification. For the first step, the rock mass was characterized using the Geological Strength Index. Next, the mass and stiffness parameters were estimated for numerical modeling using empirical equations. Modal analysis using a finite element model was then performed to determine the natural periods and mode shapes of the tunnel and the rock mass.

For the second step, the ground motion selection and modification were done following the Indonesian seismic design standard SNI 1726:2019 and SNI 8899:2020, which both referred to ASCE 7-16 and the geotechnical design standard SNI 8460:2017, which referred to the 2012 version of AASHTO LRFD Design Specifications. This process involved selecting ground motion records, generating the target response spectrum, and modifying the records. Selection criteria included magnitude and distance of the earthquake sources, structural natural period, and the site S-wave velocity. Finally, the records were modified using the amplitude scaling method. This method was chosen over the spectral matching method to preserve the characteristics of the earthquakes.

4 DETERMINATION OF NATURAL PERIODS OF THE TUNNEL

4.1 Rock Mass Characterization

The rock mass was characterized into several layers to simplify the numerical modeling. The Geological Strength Index (GSI) was used to characterize the rock mass. The GSI of the rock mass was estimated from the boring log data using Equation (1) (Hoek *et al*., 2013) and the Rock Mass Rating (RMR) on the tunnel face using Equation (2) (Hoek *et al*., 1995).

$$GSI = 1.5JCond_{89} + \frac{RQD}{2} \quad (1)$$

$$GSI = RMR_{89'} - 5 \quad (2)$$

where RQD is the Rock Quality Designation (Deere & Deere, 1988), $JCond_{89}$ is the joint condition, and $RMR_{89'}$ is the Rock Mass Rating. The $JCond_{89}$ and $RMR_{89'}$ are according to the 1989 version of the RMR classification (Bieniawski, 1989). Equation (2) cannot be used for $RMR_{89'}<23$.

In this study, BH 01 and BH 02 of the 2019 boring log data (Dharmawan, 2019) were used because they were the closest boreholes to the tunnel-fault intersection, as seen in Figure 1. Using Equation (1) and the boring log data, the GSI values on each depth below the surface were estimated. Since the boreholes didn't reach the tunnel elevation, the RMR data on the tunnel face for each 10-meter excavation span (Triristanto, 2023) were also considered. Using Equation (2), the GSI values on the tunnel face were estimated. The GSI values in BH 01, BH 02, and on the tunnel face are summarised in Figure 2.

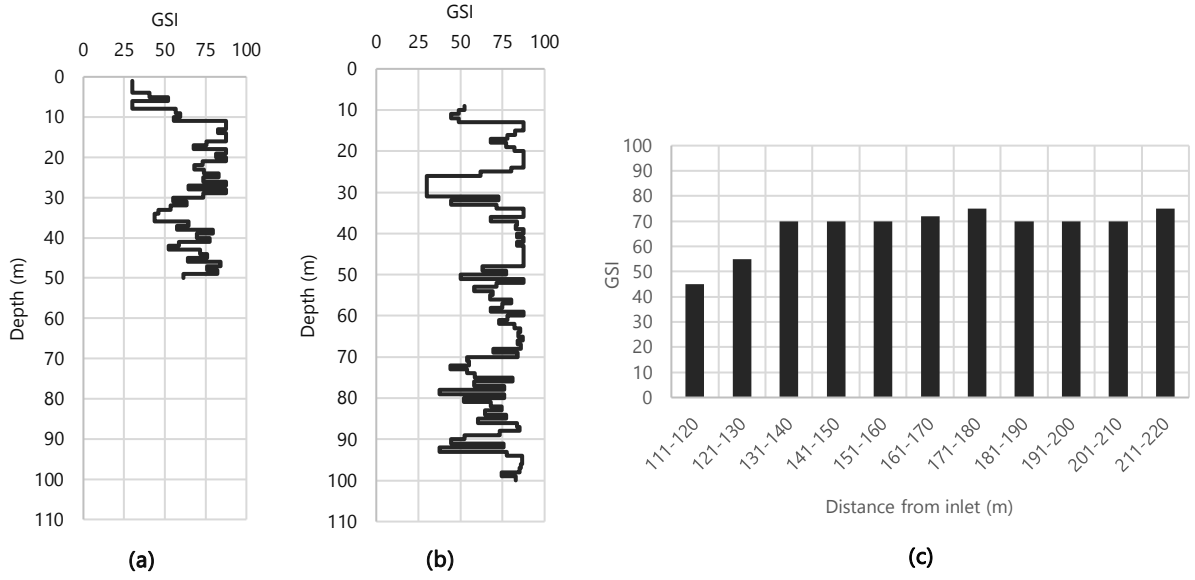

Figure 2. Estimation of GSI values at each depth of (a) BH 01, (b) BH 02, and (c) on the tunnel face.

Based on the estimation in Figure 2, the rock mass was simplified into several layers with GSI values for each layer. This was done for the numerical modelling and is summarised in Table 1. The GSI of the fault fracture zone can be estimated as "poor" or "very poor" with the GSI value of 20 (Marinos *et al*., 2007).

Table 1. Layer simplification and the GSI values of each layer.

Depth (m)	GSI value	Rock class
0 – 2	-	Residual Soil
2 – 10	36.64	Poor Rock
10 – 39	68.10	Good Rock
39 – 60	74.00	Good Rock
> 60	71.28	Good Rock

4.2 Rock Mass and Fault Parameters

To determine the natural periods using modal analysis, the mass and stiffness parameters were required. The mass properties were derived from the unit weight of the rock mass that was obtained from Dharmawan (2019). The stiffness properties of the rock mass were determined by the rock mass elastic modulus (E_{rm}) and Poisson's ratio (ν_{rm}). Those parameters were estimated using Equation (3) (Hoek & Diederichs, 2006) and Equation (4) (Narimani *et al*., 2023).

$$E_{rm} = E_i \left(0.02 + \frac{1 - \frac{D}{2}}{1 + \exp\left(\frac{60 + 15D - GSI}{11}\right)} \right) \tag{3}$$

$$\nu_{rm} = -0.002GSI + \nu_i + 0.2 \tag{4}$$

where E_i is the elastic modulus of intact rocks and ν_i is the Poisson's ratio of intact rocks. These intact rock parameters were obtained from Dharmawan (2019). The notation D means the disturbance factor and the value of D=0 for excellent quality-controlled blasting (Hoek *et al*., 2002) was used.

The stiffness properties of the fault plane were the normal stiffness (K_n) and shear stiffness (K_s) parameters. These were estimated using Equations (5) and (6) (Rocscience Inc., 2023).

$$K_n = E_0/h \tag{5}$$

$$K_s = G_0/h \tag{6}$$

where h is the thickness of infilling materials in the discontinuity. In this study, the thickness of the fracture zone was considered as the thickness of the infilling materials. The parameter E_0 was the same as E_{rm} and was obtained using Equation (3). The shear modulus (G_0) was obtained through the relationship of G_0 and E_0 in Equation (7).

$$G_0 = \frac{E_0}{2(1 + \nu)} \tag{7}$$

The thickness of the fault fracture zone was estimated from a zone in BH 01 of the 2019 boring log data that had very low RQD values and was highly weathered. The zone was estimated to be five meters and located at a depth of 27 – 32 m.

4.3 Numerical Modeling

Finite element modelling was done to conduct modal analysis. The analysis was conducted using Midas GTS NX. The geometry and boundary conditions of the model can be seen in Figure 3. The properties of each material can be seen in Table 2. The rock mass and fault properties were estimated based on Subchapter 4.2 and the tunnel properties and geometry were obtained through Bagio (2021). The residual soil layer with a unit weight of 18.6 kN/m^3 (Bagio, 2021) and a thickness of 2 m was modeled as mass elements equivalent to a pressure load of 37.2 kPa. The model's boundary conditions consisted of elastic spring elements on the bottom and side faces. The springs' modulus of subgrade reaction coefficients (k) were generated based on Equations (8) through (10) (Midas IT Co., 2024). In this model, the temporary supports, i.e., shotcrete, wire mesh, and rock bolts, were ignored. The reinforcement bars in the concrete were also ignored so that only the stiffness of the concrete was considered.

$$k = k_0 \cdot \left(\frac{B}{30}\right)^{-\frac{3}{4}} \quad (8)$$

$$k_0 = \frac{1}{30} \cdot \alpha \cdot E_0 \quad (9)$$

$$B = \sqrt{A} \quad (10)$$

where A is the cross section in vertical and horizontal directions and α is applied as 1.0.

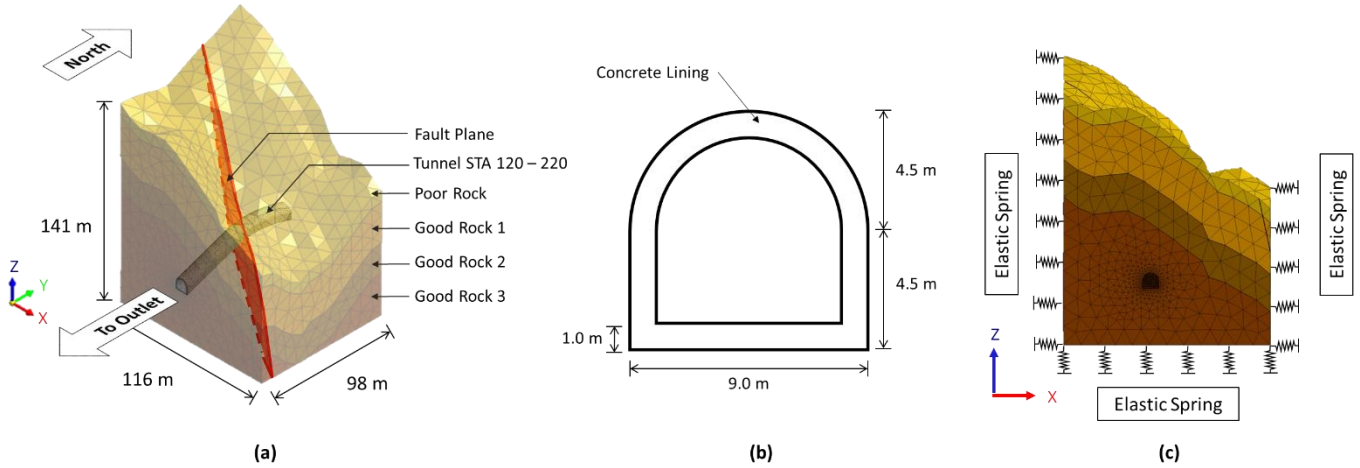

Figure 3. Geometry of (a) the rock mass, (b) the tunnel, and (c) the boundary condition of the model.

Table 2. Model material properties.

	Poor Rock	Good Rock 1	Good Rock 2	Good Rock 3	Fault Plane	Tunnel Lining
Element type	3D solid	3D solid	3D solid	3D solid	Plane interface	2D shell
Unit weight, γ(kN/m^3)	16.00	16.00	17.00	16.00	-	24.00
Elastic modulus, E (kPa)	1.95×10^5	2.97×10^6	1.09×10^6	1.33×10^6	-	2.03×10^7
Poisson's ratio, ν	0.49	0.49	0.49	0.49	-	0.15
Normal stiffness, K_n (kPa/m)	-	-	-	-	2.09×10^4	-
Shear stiffness, K_s (kPa/m)	-	-	-	-	7.00×10^3	-

4.4 Natural Periods of the Tunnel

The comparison of the first three modal periods and mode shapes of the tunnel with and without the fault is shown in Figure 4. For both models, in the first mode, translation occurred along the Z-axis. The second mode and the third mode of both models were different. For the model without fault, the second mode rotated in the Y-axis and the third mode rotated in the X-axis while for the model with fault, the second mode rotated in the X-axis and the third mode rotated in the Y-axis. The presence of the fault significantly altered the tunnel's deformation in each mode. Another distinction lay in the modal period values. The tunnel model with the fault generally exhibited higher modal periods across all modes compared to the model without the fault. For instance, in the first mode, the natural period of the tunnel without the fault was 0.582 seconds, whereas for the tunnel with the fault, it was 0.551 seconds.

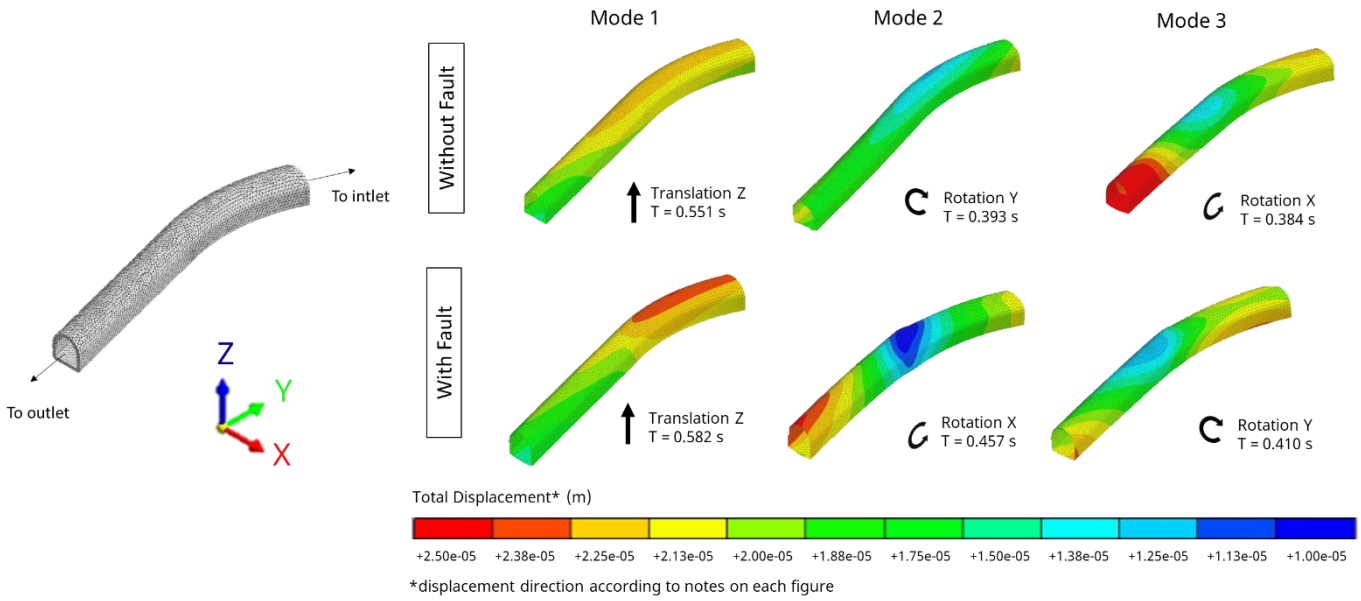

Figure 4. Comparison of the first three modes of the tunnel with and without the fault.

5 GROUND MOTION SELECTION AND MODIFICATION

5.1 Ground Motion Selection

According to SNI 1726:2019, a series of not less than 11 ground motion pairs should be selected for each target spectrum. The earthquake records need to be selected considering the site parameters. Those are earthquake magnitude, distance from earthquake sources, fault mechanism for shallow crustal earthquakes, and the S-wave velocity of the rock mass. The fault mechanism of shallow earthquake sources was obtained through the 2017 Earthquake Maps of Indonesia (National Earthquake Study Center of Indonesia, 2017). The mechanisms consisted of reverse-slip and strike-slip faults.

The earthquake magnitude and distance were obtained from Indonesian Earthquake Hazard Deaggregation Maps (National Earthquake Study Center of Indonesia, 2022). Earthquake mechanism, return period, and vibration period of the structure were required to select the maps. A return period of 1000-years was used per SNI 8460:2017 and a vibration period of 0.2 seconds was used since it was the closest to the tunnel's natural periods. The magnitudes and distances of each earthquake mechanism are summarised in Table 3.

Table 3. Magnitude and distance of each earthquake mechanism for 1000-years earthquake and vibration periods of 0.2 seconds.

Earthquake mechanism	Magnitude, M_w	Distance, R (km)
Shallow Crustal	6.0 – 6.2	30 – 40
Benioff	7.0 – 7.2	120 – 150
Megathrust	8.4 – 8.6	120 – 150

The S-wave velocity was estimated using Equation (11) (Wyering *et al.*, 2012) and Equation (12) (Salaamah *et al.*, 2018). Both equations are empirical correlations for andesite breccia rocks, which correspond with the geologic condition of the site.

$$V_s = 0.5397V_p - 193.5 \tag{11}$$

$$RQD = 0.016V_p - 14.044 \tag{12}$$

where V_p is the P-wave velocity in m/s. The V_s value was determined from the average S-wave velocity of BH 01 and BH 02 of the 2019 boring log data. The V_s was estimated to be 2215 m/s. Because of the limited available records, some compromises for V_s values were made and records with the closest V_s values were selected.

The earthquake records were obtained from the PEER Ground Motion Database (ngawest2.berkeley.edu) for shallow crustal earthquakes and the NGA-Subduction Portal (Mazzoni, 2022) for subduction earthquakes. The selected earthquake records are summarised in Table 4. The response spectra for each record are shown in Figure 5.

Table 4. List of selected ground motion records.

No.	Earthquake name	Year	Station name	Site S-wave velocity, V_s (m/s)	Magnitude, M_w	Distance, R (km)	Earthquake mechanism	
1.	Chi-Chi Taiwan-04	1999	CHY102	804.36	6.20	39.30	Shallow Crustal	Strike-slip
2.	Chi-Chi Taiwan-05	1999	HWA035	677.49	6.20	33.57	Shallow Crustal	Reverse
3.	Chi-Chi Taiwan-04	1999	TCU138	652.85	6.20	33.53	Shallow Crustal	Strike-slip
4.	Chi-Chi Taiwan-05	1999	HWA020	626.43	6.20	34.00	Shallow Crustal	Reverse
5.	Chi-Chi Taiwan-03	1999	CHY035	573.04	6.20	33.86	Shallow Crustal	Reverse
6.	Kushirooki	2004	SYARI-N	517.50	7.01	123.72	Subduction	Benioff
7.	Miyagi_Pre.Off	2011	KAWAI-N	1269.80	7.15	132.60	Subduction	Benioff
8.	SouthSanriku	2003	KUJI-S	966.80	7.03	140.07	Subduction	Benioff
9.	Tokachi-oki	2003	abashiri-g	2229.80	8.29	145.24	Subduction	Megathrust
10.	Coastal.Chile	2015	ROC1	1951.00	8.31	121.84	Subduction	Megathrust
11.	Tokachi-oki	2003	BIEI-E	771.20	8.29	146.69	Subduction	Megathrust

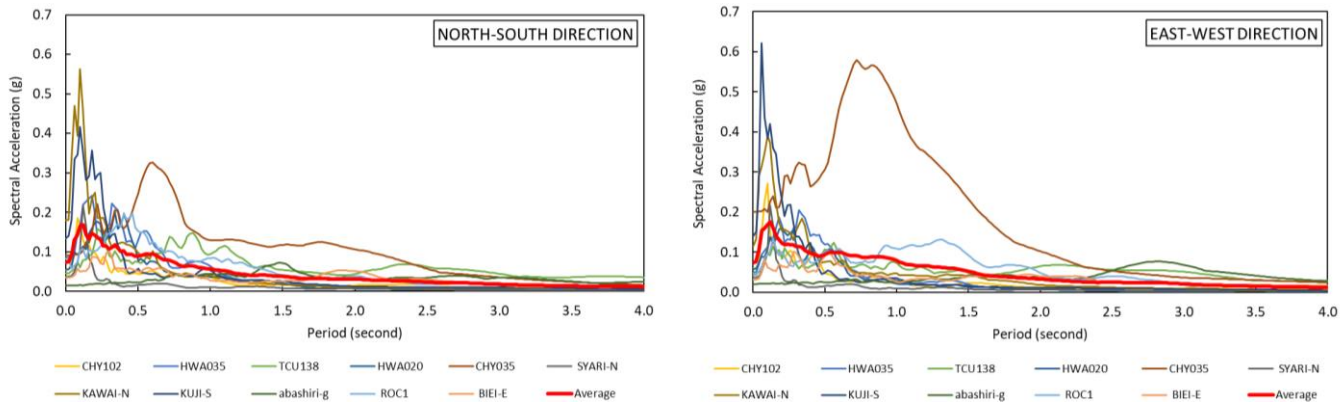

Figure 5. Response spectra of the selected ground motion records.

5.2 Ground Motion Modification

The ground motion modification was carried out following the requirements in SNI 1726:2019 and SNI 8899:2020, which govern ground motion modification for non-linear analysis according to ASCE 7-16. Each pair of horizontal ground motions must generate a maximum-direction spectrum derived from two horizontal components, applying the same scaling factor to both. The average maximum-direction spectrum should meet or exceed the target response spectrum within a defined period range and must not drop below 90% of the target response spectrum. The period range must encompass a range critical to the structure's lateral dynamic response. The upper boundary should be at least twice the largest first-mode period in the horizontal direction, while the lower boundary must include enough elastic modes to ensure 90% mass participation in each main horizontal direction and should not exceed 20% of the smallest first-mode period. For locations far from active faults, the horizontal motion components should be applied orthogonally to the structure, with the average spectral response in each direction staying within ±10% of the overall average for the given period range. SNI 8899:2020 recommended 5.0 to be the maximum scale factor.

According to the modal analysis, the first-mode period was 0.582 seconds, with 90% mass participation achieved in the third mode at a period value of 0.410 seconds. Since the structure's first mode direction was vertical, the mass participation was evaluated in that direction. The period range for modification was determined to be 0.082 - 1.164 seconds. The maximum-direction spectra of the records were established in RotD100 direction, calculated in the PEER Ground Motion Database and the NGA-Subduction Portal. The target spectrum was established based on the

guidelines outlined in SNI 8460:2017. For tunnels, the designated earthquake return period was 1000-years and the response spectrum was developed following the 2012 AASHTO guidelines. This method of generating response spectrum had also been deemed suitable for geotechnical structures in NCHRP Report 611 (Anderson *et al*., 2008). Based on the estimated V_s, the site class was classified as SA. The target spectrum was generated using APLIKASI LINI (lini.binamarga.pu.go.id), ensuring compliance with the requirements.

Table 5 displays the scale factors applied to each record, along with the peak ground acceleration (PGA) of the scaled records, as PGA is a key indicator of an earthquake's destructive potential. Figure 6 shows the maximum-direction spectra of the scaled records and the comparison of the average spectral response of each direction. It can be seen that both had satisfied the requirements.

Table 5. Scale factors and PGAs of the scaled ground motions.

No.	Earthquake name	Station name	Scale factor	PGA (g)	
				North-South (N-S) Direction	East-West (E-W) Direction
1.	Chi-Chi Taiwan-04	CHY102	5.0	0.27	0.29
2.	Chi-Chi Taiwan-05	HWA035	5.0	0.42	0.25
3.	Chi-Chi Taiwan-04	TCU138	5.0	0.22	0.24
4.	Chi-Chi Taiwan-05	HWA020	5.0	0.28	0.29
5.	Chi-Chi Taiwan-03	CHY035	2.2	0.20	0.44
6.	Kushirooki	SYARI-N	5.0	0.20	0.18
7.	Miyagi_Pre.Off	KAWAI-N	2.1	0.38	0.24
8.	SouthSanriku	KUJI-S	2.8	0.37	0.40
9.	Tokachi-oki	abashiri-g	5.0	0.07	0.10
10.	Coastal.Chile	ROC1	5.0	0.41	0.22
11.	Tokachi-oki	BIEI-E	5.0	0.17	0.16

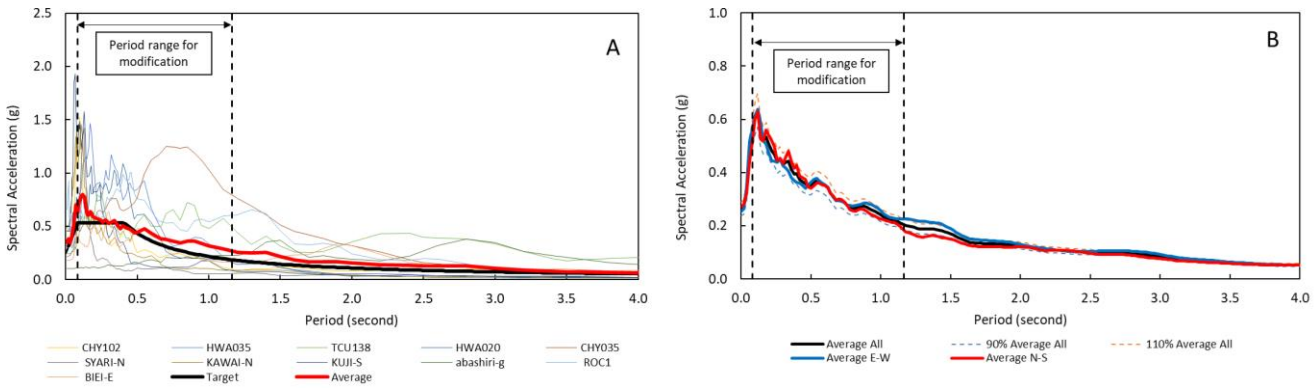

Figure 6. Maximum-direction spectra of the scaled records (A) and comparison of average spectra in each direction (B).

6 DISCUSSION

Modal analysis showed that the fault has some influence on the modal periods of the tunnel, though the effect was insignificant. Tunnels intersecting faults exhibited slightly higher modal periods due to stiffness reduction because of the fault. Although the effect was minimal, accurately determining natural periods still requires modeling the tunnel along with the surrounding rock mass and faults.

In terms of mode shape, both models exhibited similar direction in the first mode, primarily in the vertical direction due to the lower stiffness in that direction, unlike buildings where lateral movement is more critical. The second and third modes involved rotation about the X- and Y-axes due to spring supports allowing base rotation. The differences started in the second mode, where the fault-free model rotated about the Y-axis due to its sloped surface in the X-direction, while the faulted model rotated about the X-axis since the fault's strike was more parallel to this axis.

Faults also influenced deformation, particularly at the tunnel-fault intersection, where differential displacement occurred. Across all modes, the tunnel moved with the surrounding rock mass. These results emphasized the need to include the rock mass and the fault in models for accurate analysis.

Due to limited available records, some selected ground motions had S-wave velocities that didn't fully match the site conditions. These differences in S-wave velocity, especially for earthquakes recorded outside outcropping rock ($V_s \geq 750$ m/s), should be carefully considered when interpreting the dynamic analysis results. Among the selected records, CHY102 station best represented shallow crustal earthquakes, KAWAI-N was the most suitable for Benioff events, and abashiri-g for megathrust earthquakes. After scaling, the PGA values were 0.44 g at CHY035 station (shallow crustal, E-W direction), 0.40 g at KUJI-S (Benioff, E-W), and 0.41 g at ROC1 (megathrust, N-S).

7 CONCLUSION

This study demonstrated the effectiveness of modal analysis in estimating the natural periods and mode shapes of tunnels while also assessing the impact of faults. The presence of faults increased the natural period across all modes and influenced the tunnel's mode shape. For the ground motion selection, 11 pairs of ground motion records were identified, with CHY102 best representing shallow crustal earthquakes, KAWAI-N for Benioff events, and abashiri-g for megathrust earthquakes. After scaling, the highest PGA values were recorded as 0.44 g at CHY035 (shallow crustal, E-W direction), 0.40 g at KUJI-S (Benioff, E-W), and 0.41 g at ROC1 (megathrust, N-S). These findings highlight the importance of incorporating fault effects for appropriate ground motion selection and modification in tunnel seismic analysis.

REFERENCES

Amrei, S. A. R., Vahdani, R., Gerami, M., & Amiri, G. G. (2020). Correlation effects of near-field seismic components in circular metro tunnels: A case study—Tehran Metro Tunnels. *Shock and Vibration*, *2020*(1), 3016465. https://doi.org/10.1155/2020/3016465

Anderson, D. G., Martin, G. R., Lam, I. (Po), & Wang, J. N. (Joe). (2008). *Seismic analysis and design of retaining walls, buried structures, slopes, and embankements* (NCHRP Report 611). National Cooperative Highway Research Program, Transportation Research Board.

Bagio, C. A. (2021). *Analysis of the effect of fault existence on tunnel stability based on 3D numerical simulation* [Master Thesis]. Gadjah Mada University.

Bieniawski, Z. T. (1989). *Engineering rock mass classifications: A complete manual for engineers and geologists in mining, civil, and petroleum engineering*. Wiley.

Deere, D. U., & Deere, D. W. (1988). The Rock Quality Designation (RQD) index in practice. In L. Kirkaldie, *Rock classification systems for engineering purposes* (pp. 91–101). ASTM International, West Conshohocken. https://doi.org/10.1520/STP48465S

Dharmawan, A. G. (2019). *Evaluation of engineering geological conditions and stability analysis of the Bener Dam diversion tunnel, Purworejo Regency, Central Java Province* [Master Thesis]. Gadjah Mada University.

Hoek, E., Carranza-Torres, C., & Corkum, B. (2002). Hoek-Brown failure criterion – 2002 Edition. *Proc. NARMS-TAC Conference*. NARMS-TAC Conference, Toronto.

Hoek, E., Carter, T. G., & Diederichs, M. S. (2013). Quantification of the Geological Strength Index chart. *The 47th U.S. Rock Mechanics/Geomechanics Symposium*, ARMA-2013-672.

Hoek, E., & Diederichs, M. S. (2006). Empirical estimation of rock mass modulus. *International Journal of Rock Mechanics and Mining Sciences*, *43*(2), 203–215. https://doi.org/10.1016/j.ijrmms.2005.06.005

Hoek, E., Kaiser, P. K., & Bawden, W. F. (1995). *Support of underground excavations in hard rock*.

Hung, C. J., Monsees, J., Munfah, N., & Wisniewski, J. (2009). *Technical manual for design and construction of road tunnels—civil elements* (FHWA-NHI-10-034). National Highway Institute, U.S. Department of Transportation, Federal Highway Administration.

Marinos, P. G., Marinos, V., & Hoek, E. (2007). Geological Strength Index (GSI). A characterization tool for assessing engineering properties for rock masses. In C. Olalla, Á. Perucho, & M. Romana (Eds.), *Underground Works under Special Conditions: Proceedings of the ISRM Workshop W1, Madrid, Spain*. Taylor & Francis. https://doi.org/10.1201/NOE0415450287

Mazzoni, S. (2022). *NGA-Subduction Portal: Ground-motion record selection and download*. The B. John Garrick Institute for the Risk Sciences. https://doi.org/10.34948/N3D59V

Midas IT Co. (2024). *Basic tutorial: 3D moving train load time history*. Midas IT Co.

Narimani, S., Davarpanah, S. M., & Vásárhelyi, B. (2023). Estimation of the Poisson's ratio of the rock mass. *Periodica Polytechnica Civil Engineering*, *68*(1), 274–288. https://doi.org/10.3311/PPci.22689
National Earthquake Study Center of Indonesia. (2017). *Earthquake sources and hazards maps of Indonesia 2017*. Ministry of Public Works and Public Housing of the Republic of Indonesia.
National Earthquake Study Center of Indonesia. (2022). *Earthquake hazard deaggregation maps of Indonesia for earthquake-resistant infrastructure planning and evaluation*. Ministry of Public Works and Public Housing of the Republic of Indonesia.
National Standardization Agency of Indonesia. (2017). *Geotechnical design requirements* (SNI 8460:2017). National Standardization Agency of Indonesia.
National Standardization Agency of Indonesia. (2019). *Earthquake resistance planning procedures for building and non-building structures* (SNI 1726:2019). National Standardization Agency of Indonesia.
National Standardization Agency of Indonesia. (2020). *Procedures for selecting and modifying surface ground motion for earthquake-resistant building planning* (SNI 8899:2020). National Standardization Agency of Indonesia.
Rocscience Inc. (2023). *Estimating joint stiffness*. Rocscience Inc.
Salaamah, A. F., Fathani, T. F., & Wilopo, W. (2019). Correlation of P-wave velocity with Rock Quality Designation (RQD) in volcanic rocks. *Journal of Applied Geology*, *3*(2), 62-72. https://doi.org/10.22146/jag.48594
Sasangka, D. J. (2019). *Portal and excavation method stability analysis based on engineering geological conditions of the Bener Dam diversion tunnel, Purworejo Regency* [Master Thesis]. Gadjah Mada University.
Triristanto, E. R. (2021). *Engineering geological evaluation and deformation analysis of the Bener Dam diversion tunnel, Purworejo Regency, Central Java Province* [Master Thesis]. Gadjah Mada University.
Wang, J.-N. (Joe). (1993). *Seismic design of tunnels*. Parsons Brinckerhoff Inc.
Wang, Y., Jing, H., Su, H., & Xie, J. (2017). Effect of a fault fracture zone on the stability of tunnel-surrounding rock. *International Journal of Geomechanics*, *17*(6), 04016135. https://doi.org/10.1061/(ASCE)GM.1943-5622.0000837
Wyering, L., Villeneuve, M., & Wallis, I. (2012). The effects of hydrothermal alteration on mechanical rock properties of the andesite breccia and Tahorakuri Formation from the Ngatamariki Geothermal Field, New Zealand and empirical relations between rock strength and physical properties. *The 34th New Zealand Geothermal Workshop, Auckland, New Zealand.*